Biomaterials 34 (2013) 3795–3806

Contents lists available at SciVerse ScienceDirect

Biomaterials

journal homepage: www.elsevier.com/locate/biomaterials

Poly(ethylene glycol)–paclitaxel–alendronate self-assembled micelles for the targeted treatment of breast cancer bone metastases

Keren Miller [a], Chiara Clementi [b], Dina Polyak [a], Anat Eldar-Boock [a], Liat Benayoun [c], Iris Barshack [d,e], Yuval Shaked [c], Gianfranco Pasut [b], Ronit Satchi-Fainaro [a,*]

[a] Department of Physiology and Pharmacology, Sackler School of Medicine, Tel Aviv University, Tel Aviv 69978, Israel
[b] Department of Pharmaceutical and Pharmacological Sciences, University of Padova, Via F. Marzolo 5, Padova 35131, Italy
[c] Department of Molecular Pharmacology, Rappaport Faculty of Medicine, Technion, Israel Institute of Technology, 1 Efron St. Bat Galim, Haifa 31096, Israel
[d] Department of Pathology, Sackler School of Medicine, Tel Aviv University, Tel Aviv 69978, Israel
[e] Department of Pathology, Chaim Sheba Medical Center, Ramat Gan 52621, Israel

ARTICLE INFO

Article history:
Received 17 December 2012
Accepted 9 January 2013
Available online 21 February 2013

Keywords:
Angiogenesis
Polymer therapeutics
Dendrimers
Bone targeting
PEG
Alendronate

ABSTRACT

Paclitaxel (PTX) and alendronate (ALN) are effective drugs used for the treatment of breast cancer bone metastases. Growing evidence suggests that low-dose taxanes and bisphosphonates possess anti-angiogenic properties. However, PTX is water-insoluble and toxic, even if administered at anti-angiogenic dosing schedule. Polymer conjugation of PTX will increase water-solubility and improve its pharmacokinetic profile directing it to the tumor site. We further propose to combine it with ALN for active bone targeting. We conjugated ALN and PTX with poly(ethylene glycol) (PEG) forming self-assembled micelles where PTX molecules are located at the inner core and the water-soluble ALN molecules at the outer shell. PTX–PEG–ALN micelles exhibited similar *in vitro* cytotoxic and anti-angiogenic activity as the free drugs. Biodistribution analysis demonstrated preferential tumor accumulation of FITC-labeled PTX–PEG–ALN micelles. Pharmacokinetic studies revealed longer $t_{1/2}$ of the conjugate than free PTX. PTX–PEG–ALN micelles achieved improved efficacy and safety profiles over free PTX in syngeneic and xenogeneic mouse models of mCherry-infected mammary adenocarcinoma in the tibia, as monitored intravitally non-invasively by a fluorescence imaging system. The described data warrants the potential use of PTX–PEG–ALN as bone-targeted anticancer and anti-angiogenic therapy for breast cancer bone metastases.

1. Introduction

Breast cancer is the second leading cause of cancer–related deaths among women worldwide [1]. Despite extensive exploration for novel anticancer drugs or therapeutic strategies, the success of current treatments is far from satisfying, and the side effects can be particularly harsh [2,3]. Bone is an especially favored metastatic site for breast and prostate cancers. More than 25% of breast cancer patients with invasive cancer will develop bone metastases [4]. At autopsy, more than 80% of women who die from the disease show evidence of skeletal involvement [5].

Paclitaxel (PTX) has been proved to be a potent drug used to treat metastatic breast cancer, ovarian cancer, and other forms of cancer. PTX's mechanism of action on cancer cells is well known, however its anti-angiogenic activity was reported only in the last decade [6–9]. Administration of PTX at both maximum tolerated dose (MTD), that targets cancer cells and at low metronomic (anti-angiogenic) dosing schedule that targets endothelial cells is associated with several toxic side-effects and clinical complications [10,11]. In addition, due to poor water-solubility of PTX, it is formulated in Cremophor EL which causes anaphylactic and hypersensitivity reactions [11]. Therefore, potential therapeutic strategies to improve the efficacy of PTX and reduce its side effects are needed.

The aminobisphosphonate, alendronate (ALN) has emerged in recent years as a highly effective therapeutic option for the prevention of skeletal complications caused by bone metastases. Although ALN is mostly known for its potent antiresorptive activity due to specific osteoclasts induction of apoptosis, it also demonstrates anticancer and anti-angiogenic activity [12–14]. Like all bisphosphonates, it exhibits exceptionally high affinity to the bone-mineral hydroxyapatite (HA) [12,14–16]. Because of the high bone affinity of bisphosphonates, much effort has been made to

* Corresponding author. Tel.: +972 3 640 7427; fax: +972 3 640 9113.
E-mail address: ronitsf@post.tau.ac.il (R. Satchi-Fainaro).

0142-9612/$ – see front matter © 2013 Elsevier Ltd. All rights reserved.
http://dx.doi.org/10.1016/j.biomaterials.2013.01.052

conjugate them with non-specific bone therapeutic agents in order to obtain osteotropicity [16–18]. Recently, ALN was successfully conjugated with polymeric drug delivery systems [15,19,20].

Here, we developed an approach which attempts to target PTX selectively to bone metastases, thus reducing its side effects, improving its pharmacokinetics, modifying its biodistribution and enhancing its efficacy. Our strategy rests upon the conjugation of the specific bone targeting moiety ALN, and PTX with poly(ethylene glycol) (PEG) bearing a β-Glutamic acid dendron at one end of the polymeric backbone, as an aim to increase the loading of ALN.

We have previously shown that an HPMA copolymer-PTX–ALN conjugate enhanced the anti-angiogenic and anticancer effect of the free drugs, and reduced their toxicities [20,21]. ALN facilitated the delivery of PTX to the bones. Here, we hypothesized that the conjugation with PEG, similar to HPMA copolymer, would target PTX mostly to the metastatic sites within the bones and scarcely to normal healthy bones, due to the enhanced permeability and retention (EPR) effect, by virtue of its size [22].

The water-soluble PEG is a non-toxic, non-immunogenic, and commercially-available FDA-approved polymer [23]. Furthermore, conjugation with PEG should restrict the passage through the blood brain barrier thus abrogating neurotoxicity associated with free PTX and would prolong the circulating half-life of the free drugs ALN and PTX. Consequently, the inhibitory effect on the growth of tumor endothelial and epithelial cells would be enhanced, by exposing the cells to the conjugated drugs in the circulation for a longer time [24–26]. Furthermore, to achieve stronger targeting to the bone, we designed and synthesized a PTX–PEG–ALN conjugate with an increased loading of ALN molecules per polymer chain. This approach yields a conjugate with a well-defined chemical structure resulting in improved batch to batch reproducibility and biological outcomes [27,28].

We previously reported the design, synthesis and physicochemical characterization of PTX–PEG–ALN that showed a marked affinity for the bone mineral HA and an IC_{50} towards human prostate cancer cells (PC3) comparable to that of the free drugs combination [29]. Here, we evaluated the anti-angiogenic and anticancer activity *in vitro* and *in vivo*, the biodistribution and pharmacokinetics of FITC-labeled PTX–PEG–ALN conjugate.

2. Materials and methods

2.1. Materials

PTX and ALN were purchased from Alcon Biosciences Ltd. (Mumbai, India; Petrus Chemicals and Materials Ltd., Israel). Dulbecco's modified Eagle's medium (DMEM), RPMI 1640, Fetal bovine serum (FBS), Penicillin, Streptomycin, Nystatin, L-glutamine, Hepes buffer, sodium pyruvate, and fibronectin were from Biological Industries Ltd. (Kibbutz Beit Haemek, Israel). EGM-2 medium was from Cambrex (Walkersville, MD, U.S.A). Matrigel matrix was from BD Biosciences, USA. Peroxidase Block was purchased from Merck, Germany. Primary rat anti-murine CD34 antibody (MEC 14.7) was from Abcam, (Cambridge, MA). Rabbit anti-rat antibody, anti-rabbit horseradish peroxidase-conjugated antibody (ABC detection kit) and ImmPACT™ DAB diluent kit were from Vector Laboratories (Burlingame, CA, USA). pEGFPLuc plasmid was from Clontech (Mountain View, CA, USA). Nuclear staining was from Procount, BD Pharmingen (San Jose, CA, USA). 7-aminoactinomycin D (7AAD) was from Chemicon (Billerica, MA). Dextran (MW ~70,000) and all other chemical reagents, including salts and solvents were purchased from Sigma–Aldrich, Israel. All reactions requiring anhydrous conditions were performed under an $Ar_{(g)}$ or $N_{2(g)}$ atmosphere. Chemicals and solvents were either A.R. grade or purified by standard techniques.

2.2. Synthesis of PTX–PEG, PEG–ALN, PTX–PEG–ALN and FITC labeled conjugates

The conjugates were synthesized and characterized in terms of their drug loading and hydrodynamic diameter as previously described [29]. Synthesis of FITC-labeled conjugates was performed exploiting the same chemical strategy for the preparation of non-labeled conjugates. The new steps are described in the supplemental materials.

2.3. Cell culture

MDA-MB-231 human mammary adenocarcinoma and 4T1 murine mammary adenocarcinoma cell lines were purchased from the American Type Culture Collection (ATCC). MDA-MB-231 cells were cultured in DMEM supplemented with 10% FBS, 100 μg/ml Penicillin, 100 U/ml Streptomycin, 12.5 U/ml Nystatin and 2 mM L-glutamine. 4T1 cells were cultured in RPMI 1640 supplemented with 10% FBS, 100 μg/ml Penicillin, 100 U/ml Streptomycin, 12.5 U/ml Nystatin, 2 mM L-glutamine, 10 mM Hepes buffer, and 1 mM sodium pyruvate. Human umbilical vein endothelial cells (HUVEC) were obtained from Cambrex (Walkersville, MD, U.S.A) and grown according to the manufacturer's protocol in EGM-2 medium (Cambrex). Cells were grown at 37 °C; 5% CO_2.

2.4. Generation of mCherry-infected human MDA-MB-231 and murine 4T1 mammary adenocarcinoma cell lines

4T1 and MDA-MB-231 cells were infected with mCherry as previously described [19].

2.5. Cell viability assay

HUVEC were plated onto 24-well plate (1.5×10^4 cells/well) in growth factors reduced media, (EBM-2, Cambrex, USA) supplemented with 5% FBS. Following 24 h of incubation (37 °C; 5% CO_2), medium was replaced with EGM-2 (Cambrex, USA). 4T1 and MDA-MB-231 cells were plated onto 96 well plate (5×10^3 cells/well) in DMEM or RPMI, respectively, supplemented with 5% FBS and incubated for 24 h (37 °C; 5% CO_2). Following 24 h of incubation, medium was replaced with DMEM, or RPMI containing 10% FBS. Cells were challenged with the combination of free PTX plus ALN, each free drug alone, and with PEG, PEG–ALN, PTX–PEG, and PTX–PEG–ALN conjugates at serial concentrations for up to 72 h. Following incubation, HUVEC were counted by Coulter Counter. 4T1 and MDA-MB-231 cells viability was measured using the MTT assay.

2.6. Capillary-like tube formation assay

The surface of 24-well plates was coated with Matrigel matrix (50 μL/well) (BD Biosciences, USA) on ice and was then allowed to polymerize at 37 °C for 30 min. HUVEC (3×10^4) were challenged with the combination of free PTX (5 nM) plus ALN (23 nM), each drug alone, and with PEG, PEG–ALN, PTX–PEG and PTX–PEG–ALN conjugates at equivalent concentrations, and were seeded on coated plates in the presence of complete EGM-2 medium. After 8 h of incubation (37 °C; 5% CO_2), wells were imaged using Nikon TE2000E inverted microscope integrated with Nikon DS5 cooled CCD camera by 4× objective, brightfield technique.

2.7. Migration assay

Cell migration assay was performed using modified 8 μm Boyden chambers Transwells® (Costar Inc., USA) coated with 10 μg/ml fibronectin (Biological industries, Beit Haemek, Israel). HUVEC (15×10^4 cells/100 μL) were challenged with the combination of PTX (100 nM) plus ALN (460 nM), each drug alone, and with PEG, PEG–ALN, PTX–PEG, and PTX–PEG–ALN conjugates at equivalent PTX and ALN concentrations, and were added to the upper chamber of the transwells for 2 h incubation prior to migration to vascular endothelial growth factor (VEGF). Following incubation, cells were allowed to migrate to the underside of the chamber for 4 h in the presence or absence of VEGF (20 ng/mL) in the lower chamber. Cells were then fixed and stained (Hema 3 Stain System; Fisher Diagnostics, USA). The stained migrated cells were imaged using Nikon TE2000E inverted microscope integrated with Nikon DS5 cooled CCD camera by 10× objective, brightfield illumination. Migrated cells from the captured images per membrane were counted using NIH image software. Migration was normalized to percent migration, with 100% representing migration to VEGF alone.

2.8. Measurement of circulating endothelial cells (CEC) and circulating endothelial progenitor (CEP) by flow cytometry

Blood was obtained from anaesthetized mice by retro-orbital sinus bleeding. CEC and CEP were quantitated using flow cytometry, as described previously [30]. Briefly, 24 h after treatment, blood was collected in tubes containing EDTA to avoid clotting. Monoclonal antibodies were used to detect CEC and CEP population with the following antigenic phenotypes: CD13+/VEGFR2+/CD45−/dim. CEP population was also CD117+. Nuclear staining was used in some experiments to exclude platelets or cellular debris. 7-aminoactinomycin D (7AAD) was used to distinguish apoptotic and dead cells from viable cells. After red cell lysis, cell suspensions were analyzed and at least 200,000 cells per sample were acquired. Analyses were considered informative when an adequate number of events (i.e. >50, typically 50–150) were collected in the CEC and CEP enumeration gate in untreated control animals. Percentages of stained cells were determined and compared with appropriate negative controls. Positive staining was defined as being greater than non-specific background staining. Flow cytometry studies were performed on Cyan ADP flow

cytometer (Beckman Coulter) and analyzed with Summit (Beckman Coulter) software. All monoclonal antibodies were purchased from BD Biosciences and used for flow cytometry analysis in accordance with the manufacturer's protocols. Data is expressed as mean ± standard error of the mean (s.e.m.).

2.9. Evaluation of antitumor activity of PTX–PEG–ALN conjugate

A syngeneic mouse model of mammary adenocarcinoma was established by injecting Balb/c female mice with 100 μl of 4×10^5 mCherry-labeled 4T1 cells intra-tibia. Therapy was initiated one day following tumor cells inoculation. Mice were randomly divided into 9 groups ($n = 6$ mice/group) and intravenously (*i.v.*) injected with 100 μl PTX (15 mg/kg), ALN (35 mg/kg), combination of free PTX plus ALN, PEG, PTX–PEG, PEG–ALN, or PTX–PEG–ALN conjugates at equivalent concentrations, and PTX-vehicle (1:1:8 Ethanol:Cremophor EL:Saline) or saline that were used as controls. A xenograft mouse model was established by injecting 100 μl of 1×10^5 mCherry-labeled MDA-MB-231 cells intra-tibia to female SCID mice. Therapy was initiated 10 days following tumor inoculation, when mice displayed fluorescent signals indicating tumors uptake. Mice were divided into 5 groups ($n = 6$ mice/group) and the mean fluorescence intensity was approximately similar for all groups. These groups were randomly assigned and administered *i.v.* with 100 μl PTX (15 mg/kg) plus ALN (35 mg/kg), PTX (7.5 mg/kg) plus ALN (17.5 mg/kg), PTX–PEG–ALN conjugate at equivalent concentration, and controls of PTX-vehicle, or saline. All treatments for both mouse models were injected *i.v.* via the tail vain, every other day for 5 injections. Tumor progression was monitored by CRI™ Maestro non-invasive intravital imaging system. At termination, tibias were removed and analyzed. Data was expressed as mean ± s.e.m.

2.10. White Blood Cell (WBC) counts

Blood was obtained from anaesthetized mice by retro-orbital sinus bleeding. Twenty four hours after treatment, blood was collected in tubes containing 0.1 M EDTA to avoid clotting. Samples were counted no longer than 5 min after blood was drawn from mice. Ten μl of blood samples were mixed with 90 μl of track solution (1% acetic acid in DDW), and cells were counted by a Z1 Coulter® Particle Counter (Beckman Coulter™). Data was expressed as mean ± s.e.m.

2.11. Immunohistochemistry

Immunohistochemistry of tumors in the tibia was performed using samples fixed with 4% paraformaldehyde, following decalcification in EDTA and paraffin embedding by the standard procedure. Paraffin sections of 4 μm were deparaffinized, rehydrated, and stained by hematoxylin and eosin (H & E). For CD34 staining, slides were deparaffinized and pre-treated with 10 mM citrate, pH 6.0 for 20 min in a steam pressure cooker (Decloaking Chamber, BioCare Medical, Walnut Creek, CA). All further steps were performed at RT in a hydrated chamber. Slides were covered with Peroxidase Block (Merck, Germany) for 10 min to quench endogenous peroxidase activity, followed by incubation with 2% of horse serum in 50 mM Tris–HCl, pH 7.4, for 30 min to block non-specific binding sites. Primary rat anti-murine CD34 antibody (MEC 14.7 1:50 dilution; Abcam, Cambridge, MA) was applied in 1% rabbit serum albumin in Tris–HCl, pH 7.4 at 4 °C overnight. Slides were washed in 50 mM Tris–HCl, pH 7.4 and rabbit anti-rat antibody (1:750 dilution; Vector Laboratories, CA, USA) was applied for 30 min. Following further washing, immunoperoxidase staining was developed using HistoMark TrueBlue peroxidase system (KPL, USA) per the manufacturer instructions and counterstained with safranin. Microvessel density (MVD) was calculated as previously described [31].

2.12. Body distribution of FITC-labeled PEG, PTX–PEG, PEG–ALN and PTX–PEG–ALN conjugates

SCID mice bearing MDA-MB-231 tumors in the tibia were injected *i.v.* with FITC-labeled PEG, PTX–PEG, PEG–ALN and PTX–PEG–ALN conjugates. Accumulation of the conjugates in the tumor was assessed at different time points (0, 2, 4, 6, and 8 h). At termination (after 8 h), tumors, organs and bones were excised and imaged. Organs were imaged using non-invasive imaging system (CRI Maestro™). Fluorescence was determined using defined regions of interest (ROI) measurements on tumors and other tissues. Time dependent tumor contrast profile was determined by the ratio between fluorescence intensities of tumors and those of normal skin. Data were expressed as mean ± standard deviation (s.d.) ($n = 3$).

2.13. Pharmacokinetic of PTX, PTX–PEG and PTX–PEG–ALN in mice

Thirty female Balb/C mice (23–25 g) were randomly divided in three groups of 10 animals. 150 μL of PTX in 1:1:8 Ethanol:Cremophor EL:Saline, PTX–PEG in PBS pH 6 or PTX–PEG–ALN in PBS pH 6 (dose: 10 mg/kg PTX equiv.) were administered via the tail vein to mice anaesthetised with 5% isoflurane gas (mixed with O_2 in enclosed cages). Blood samples of 150 μL were withdrawn from the retro-orbital plexus/sinus of the animal from 3 min to 24 h. The blood was centrifuged at 1500 *g* for 15 min. To 50 μL of plasma, 350 μL of CH_3CN was added for protein precipitation and the resulting mixture was centrifuged at 20,000 *g* for 5 min. Three hundred microliter of the supernatant was collected and freeze-dried. The residue was dissolved in 50 μL of CH_3OH and analyzed by RP-HPLC under the conditions reported above. For PTX–PEG and PTX–PEG–ALN, the residues after freeze-drying were also hydrolyzed with NaOH 2N to release the PTX before HPLC analysis.

2.14. Ethics statement

All animal procedures were performed in compliance with Tel Aviv University, Sackler School of Medicine guidelines and protocols approved by the Institutional Animal Care and Use Committee (IACUC). Body weight and tumor size were measured three times a week.

2.15. Statistical methods

In vitro data is expressed as mean ± s.d. *In vivo* data is expressed as mean ± s.e.m. Statistical significance was determined using an unpaired *t*-test. $P < 0.05$ was considered statistically significant. All statistical tests were two-sided.

3. Results

3.1. Structures of FITC-labeled PTX–PEG, PEG–ALN, PTX–PEG–ALN conjugates

The chemical structures of FITC-labeled PEG–ALN, PTX–PEG, and PTX–PEG–ALN are presented in Fig. 1. Batches of conjugates synthesized for this study revealed similar physico-chemical properties as reported for previous non-labeled batches [29]. Detailed description of the synthesis is provided in the supplemental materials section.

3.2. Evaluation of PTX–PEG–ALN conjugate anti-proliferative effect on murine 4T1 and human MDA-MB-231 adenocarcinoma of the mammary cell lines

To evaluate whether PTX and ALN retained their cytotoxic activity following conjugation with PEG polymer, a proliferation assay of 4T1 and MDA-MB-231 cells was performed. The proliferation of 4T1 cells was inhibited in a similar manner by all PTX formulations, exhibiting an IC_{50} of ~10 nM, and ~20 nM for combination of free PTX plus ALN and PTX–PEG–ALN conjugate, respectively (Fig. 2A). The proliferation of MDA-MB-231 cells was also inhibited by all PTX formulations, exhibiting an IC_{50} of ~1 nM, and ~10 nM for combination of free PTX plus ALN, and PTX–PEG–ALN conjugate, respectively (Fig. 2B).

PEG–β–Glutamic acid dendron served as control and was non-toxic at all the concentrations tested. ALN alone was found to be toxic only at the highest concentration tested of 10 μM, however ALN bound to PEG at equivalent concentration was not toxic at all the concentrations tested.

3.3. Comparing the anti-angiogenic properties of PTX–PEG–ALN conjugate to PTX

In order to assess whether, similarly to PTX, PTX–PEG–ALN conjugate possesses anti-angiogenic properties, we carried out endothelial cell proliferation, capillary-like tube formation and migration assays using the conjugates. Human umbilical vein endothelial cells (HUVEC) were incubated with the different compounds. The proliferation of HUVEC was inhibited similarly by all PTX-containing formulations, exhibiting an IC_{50} of ~2 nM, and ~4 nM for the combination of free PTX plus ALN, and PTX–PEG–ALN conjugate, respectively (Fig. 3A).

Next, the effect of PTX–PEG–ALN conjugate on the ability of HUVEC to migrate towards VEGF was evaluated. The migration of HUVEC incubated with both PTX–PEG and PTX–PEG–ALN conjugates and the combination of free PTX plus ALN towards VEGF was inhibited by ~80% (Fig. 3B).

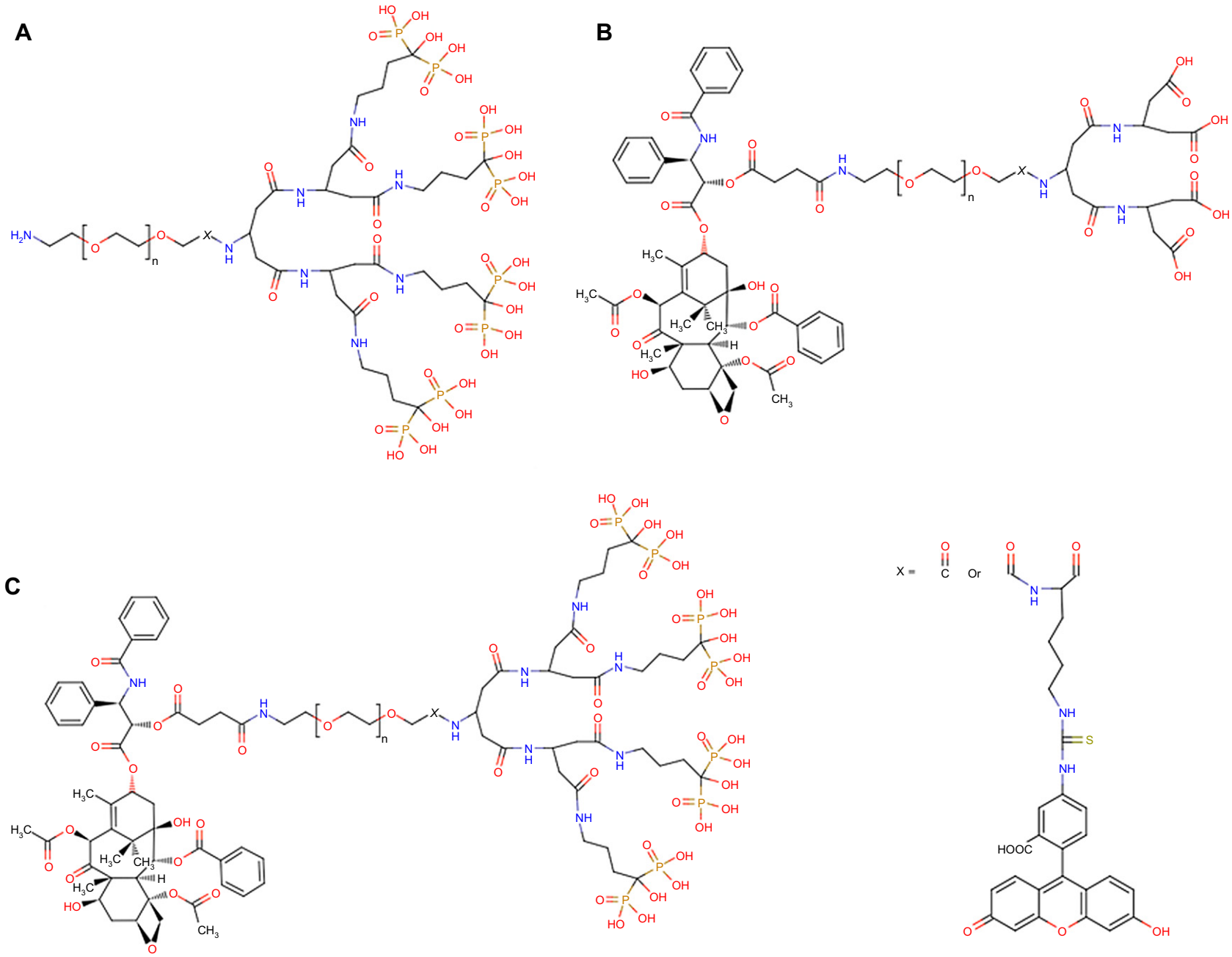

Fig. 1. Chemical structure of FITC labeled (A) PEG–ALN (B) PTX–PEG and (C) PTX–PEG–ALN.

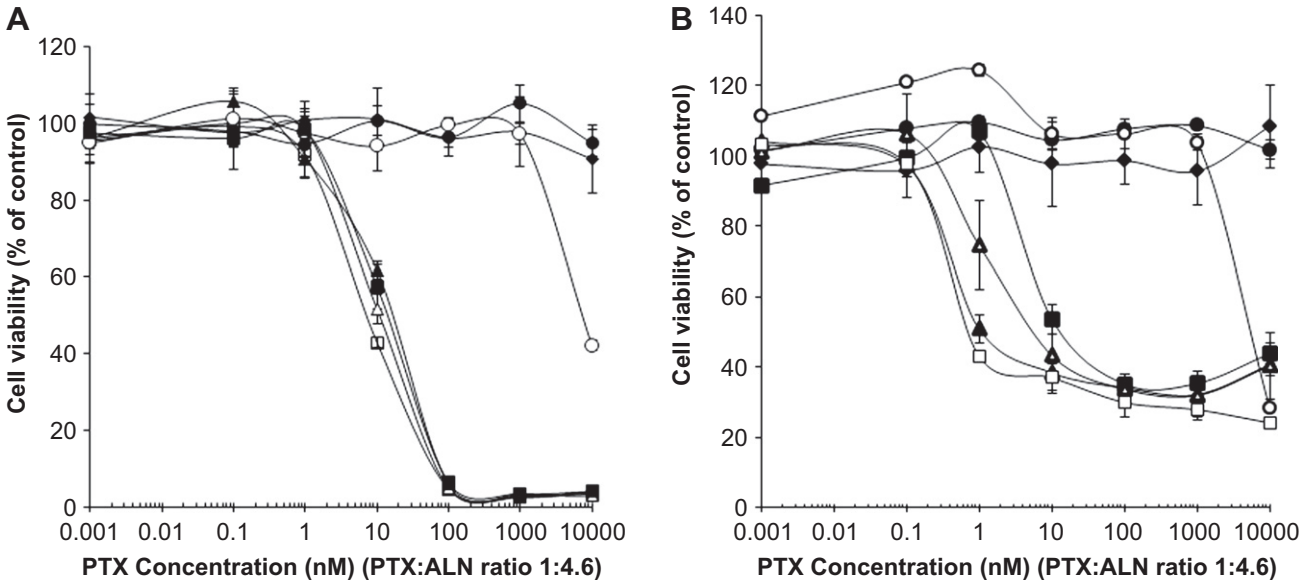

Fig. 2. PTX-PEG–ALN conjugate inhibits the proliferation of murine 4T1 and human MDA-MB-231 mammary adenocarcinoma cell lines. 4T1 (A) and MDA-MB-231 (B) cells were incubated with the combination of free PTX plus ALN (open squares), PTX (open triangles), ALN (open circles), and equivalent concentrations of PEG (close diamonds), PTX–PEG–ALN (close squares), PTX–PEG (close triangles) and PEG–ALN (close circles) conjugates for 72 h. Data represents mean ± s.d. *X*-axis is presented at a logarithmic scale.

Subsequently, we examined the effect of the conjugates on the ability of HUVEC to form capillary-like tube structures on Matrigel, an additional crucial step in the angiogenic cascade of events (Fig. 3C).

The combination of PTX plus ALN inhibited the formation of tubular structures of HUVEC by ~60%. Both PTX–PEG and PTX–PEG–ALN conjugates at PTX-equivalent concentrations inhibited the formation of the tubular structures of HUVEC by ~50% (Fig. 3D). The concentrations of treatments used in both migration and capillary-like tube formation assays on HUVEC were tested and found to be non-cytotoxic at the indicated incubation times, but rather specifically inhibited their ability to migrate and form capillary-like vascular networks.

3.4. In vivo tumor accumulation, body distribution and pharmacokinetics

Non-invasive intravital fluorescence imaging technology was utilized to monitor the real-time distribution, and tumor accumulation of FITC-labeled PEG, PTX–PEG, PEG–ALN and PTX–PEG–ALN conjugates that were injected *i.v.* to mice bearing mCherry-labeled MDA-MB-231- mammary tumors in the tibia. Immediately following administration of the conjugates, mice became entirely fluorescent. A semi-quantitative time-dependent tumor/background contrast profile was derived from the average fluorescence intensities of equal areas within tumor and normal skin regions. The FITC-labeled conjugates accumulated gradually and preferentially at tumor sites (Fig. 4A). At 8 h post injection, tumors and major organs were excised for *ex vivo* imaging to determine tissue distribution (Fig. 4B). In all conjugates, apart for tumors, uptake was predominant in kidney tissues due to renal excretion. Preferential accumulation in bones was obvious only in PEG–ALN–FITC and PTX–PEG–ALN–FITC conjugates, indicating that ALN in the conjugated form retained its binding capacity to bone mineral. The pharmacokinetics of PTX–PEG–ALN and PTX–PEG were determined in mice and compared to that of free PTX. Immediately following injection, high levels of free PTX in the serum were recorded, however following 3 min, its levels were decreased dramatically and became non-detectable at 60 min. The elimination half-lives ($T_{1/2\beta}$) of PTX–PEG and PTX–PEG–ALN were 77.9 min and 85.5 min, respectively (Fig. 4C), which is a marked prolongation with respect to the 15.1 min of free PTX. Consequently, also the area under the curve (AUC) of PTX–PEG and PTX–PEG–ALN was increased resulting in 13- and 30-fold larger than the AUC of free PTX, respectively (Fig. 4C).

3.5. Anti-tumor efficacy and toxicity of PTX–PEG–ALN conjugate on syngeneic 4T1-mCherry murine mammary adenocarcinoma in the tibia

The antitumor effect of PTX–PEG–ALN conjugate following *i.v.* administration was evaluated on syngeneic mCherry-labeled 4T1 murine mammary adenocarcinomas in the tibia. A significant tumor growth inhibition was recorded in mice treated with both PTX–PEG and PTX–PEG–ALN conjugates. On day 15, when mice were euthanized, PTX–PEG–ALN and PTX–PEG conjugates inhibited tumor growth by 48% and 37%, respectively, as compared with saline-treated mice (Fig. 5A, B). Treatment with both free ALN and combination of free ALN plus PTX was very toxic and caused severe body weight loss and mortality within 2 injections (Fig. 5C). Therefore, in these groups, tumor progression could not be determined. In contrast, mice treated with PEG–ALN or PTX–PEG–ALN conjugates did not lose weight. Further body weight loss was not recorded in any of the other treatments (Fig. 5C). WBC counts of mice treated with free PTX were significantly decreased as opposed to saline- or conjugates'-treated mice (Fig. 5D). Due to the severe toxic effects of free ALN and the combination of free ALN plus PTX, that caused mortality prior to day 11, there is no data concerning the WBC counts from these mice.

Representative histology sections of H & E staining demonstrated that most of the PEG conjugates treated-mice had intact cortical and trabecular bone (Fig. 5E). However, in the control groups and in mice treated with PTX, tumors filled the bone marrow space and destroyed both trabecular and cortical tibia bone. Increased percent necrosis was observed in control groups of mice due to the larger size of tumors incorporating a necrotic hypoxic core, as compared with smaller tumors and decreased percent necrosis observed in all treated groups of mice. Following the *in vitro* results demonstrating the anti-angiogenic activity of PTX–PEG–ALN conjugate, we performed immunohistochemical analysis

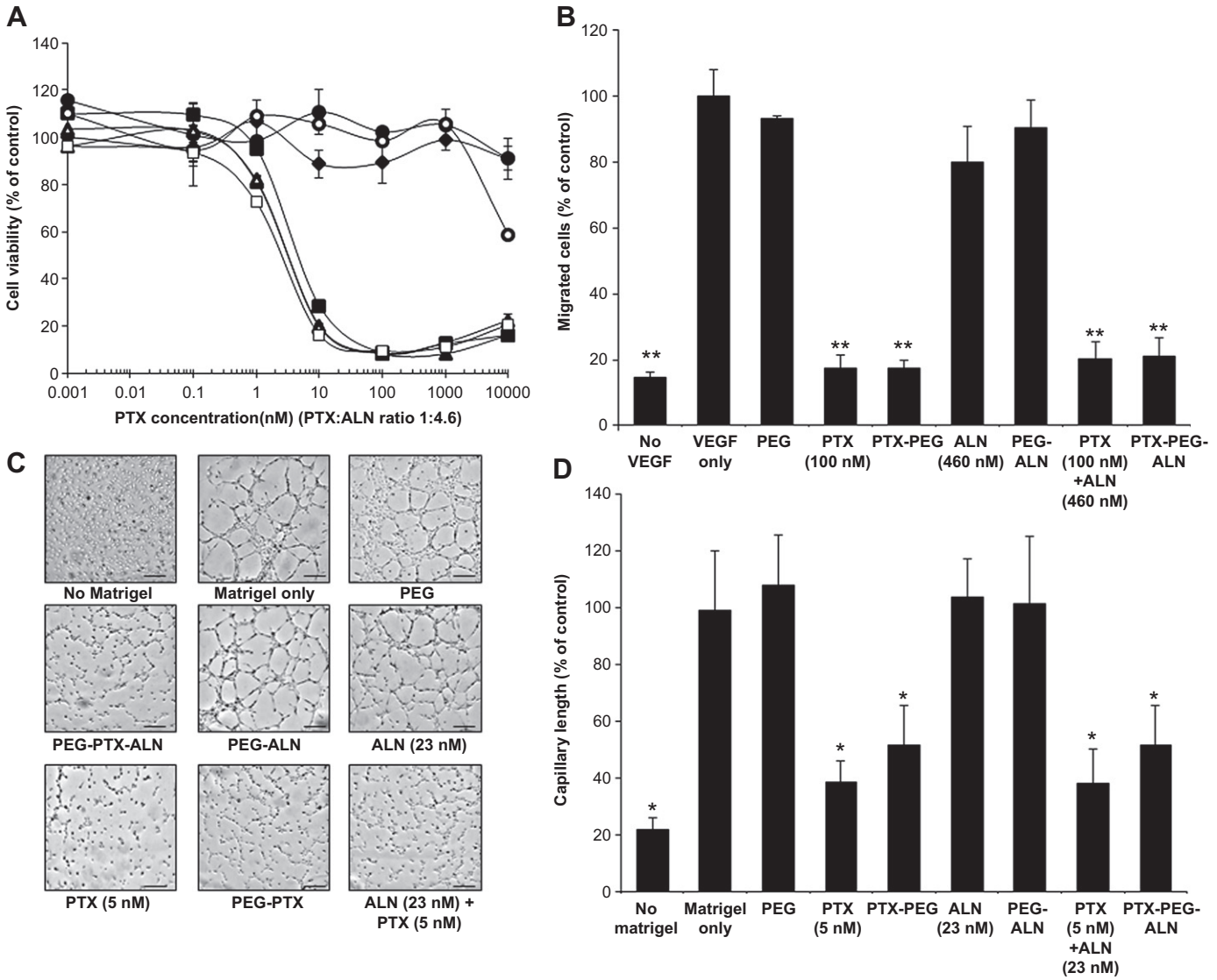

Fig. 3. PTX–PEG–ALN conjugate inhibits steps in the angiogenic cascade. HUVEC were incubated with the combination of free PTX plus ALN (open squares), PTX (open triangles), ALN (open circles), and equivalent concentrations of PEG (close diamonds), PTX–PEG–ALN (close squares), PTX–PEG (close triangles) and PEG–ALN (close circles) conjugates. (A) PTX–PEG–ALN and PTX–PEG conjugates inhibit the proliferation of HUVEC. *X*-axis is presented at a logarithmic scale. (B) PTX–PEG–ALN and PTX–PEG conjugates inhibit the migration of HUVEC towards the chemoattractant VEGF. Migration was normalized to percent migration with 100% representing migration to VEGF alone. The quantitative analysis of the number of migrated cells is presented. (C, D) PTX–PEG–ALN and PTX–PEG conjugates inhibit the ability of HUVEC to form capillary-like tube structures. (C) Representative images of capillary-like tube structures of HUVEC seeded on Matrigel following treatment (scale bar represents 100 μm). (D) Quantitative analysis of the mean length of the tubes. Data represents mean ± s.d. $^{*}P < 0.05$, $^{**}P < 0.01$.

of paraffin-embedded sections of CD34 staining. A significant reduction of ~50% in the microvessel density (MVD) was demonstrated in mice treated with PTX, PTX–PEG, and PTX–PEG–ALN, as compared with saline control treatment (Fig. 5F).

We next analyzed both CEC and CEP populations in blood circulation. Multi-parametric flow cytometry analysis revealed that mice treated with PTX–PEG–ALN conjugate displayed a significant increase in the apoptotic CEC counts in the blood (Fig. 6A). Furthermore, we observed an increase in viable CEP following PTX therapy as opposed to all other treatments (Fig. 6B).

3.6. Anti-tumor efficacy and toxicity of PTX–PEG–ALN conjugate on a xenograft model of mCherry-labeled MDA-MB-231 mammary adenocarcinoma in the tibia

The antitumor effect of PTX–PEG–ALN conjugate following *i.v.* injections was also evaluated on a xenograft mouse model of mCherry-labeled MDA-MB-231 human mammary adenocarcinoma in the tibia. PTX–PEG–ALN conjugate exhibited superior antitumor efficacy, exhibiting 50% inhibition of tumor growth, as compared to saline-treated control mice (Fig. 7A, B).

In addition, the conjugate did not induce body weight loss (Fig. 7C). However, combination of MTD of free PTX plus ALN was very toxic and induced mortality within one treatment. Also, treatment with half-dose of the combination of free PTX plus ALN was very toxic and caused severe body weight loss that almost reached 20% decrease, but was recovered after treatment withdrawal (Fig. 7C). WBC counts of mice treated with the conjugate or combination of the free drugs were comparable to control mice treated with saline or PTX-vehicle (Fig. 7D).

Representative H & E staining of paraffin-embedded sections of mCherry-labeled MDA-MB-231 tumors in the tibia demonstrated that tumors resected from control mice filled the bone marrow, destroyed the bone, and penetrated into soft tissues and the

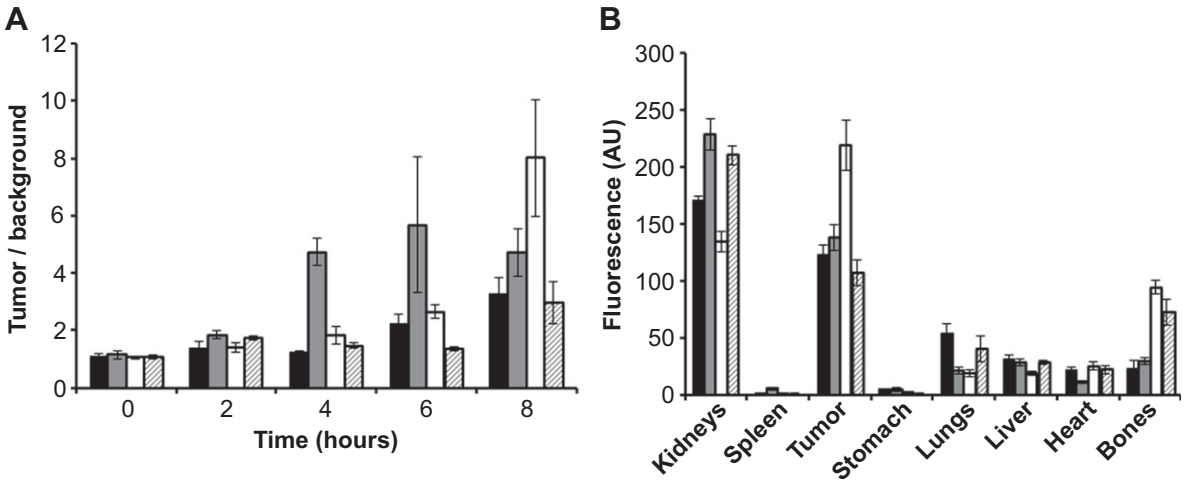

C

Parameter	PTX	PTX-PEG	PTX-PEG-ALN
$T_{½\alpha}$ (min)	1.3 ± 0.3	7.5 ± 0.6	18.9 ± 0.8
$T_{½\beta}$ (min)	15.1 ± 4.8	77.9 ± 4.0	85.5 ± 19.8
$AUC^{0-\infty}$ (μg min/mL)	31.2 ± 9.2	407.3 ± 70.7	948.4 ± 119.2
Clearance (mL/min)	7.4 ± 1.5	0.56 ± 0.08	0.24 ± 0.03
Vd (mL)	160.9 ± 2.1	63.4 ± 6.2	29.9 ± 5.5

Fig. 4. *In vivo* and *ex vivo* biodistribution of FITC labeled PEG, PTX–PEG, PEG–ALN and PTX–PEG–ALN conjugates. SCID mice bearing MDA-MB-231 tumors in the tibia were injected *i.v.* with FITC labeled PEG (black), PTX–PEG (gray), PTX–PEG–ALN (white), and PEG–ALN (stripes). Mice and organs were imaged using the fluorescence imaging system (CRI™ Maestro). (A) Semi-quantitative time dependent tumor accumulation profile of FITC-labeled conjugates. Compound's accumulation in the tumor was assessed as tumor/background (normal skin) ratios of florescence intensities of representative regions of interest. (B) *Ex vivo* fluorescence intensities of tumors and organs resected following 8 h post administration of FITC-labeled conjugates. (C) Prolonged blood circulation of PTX–PEG–ALN conjugate. Summary of the pharmacokinetic parameters obtained from female Balb/C mice that were injected with PTX (10 mg/kg), PTX–PEG or PTX–PEG–ALN conjugates at PTX equivalent concentration. Data represents mean ± s.e.m.

proximal joint. In contrast, mice treated with PTX–PEG–ALN conjugate had intact cortical and trabecular bone (Fig. 7E). Also, in this mouse model, an overall increased percent necrosis due to larger size of tumors with hypoxic core was observed in control groups of mice, as compared with smaller tumors, and decreased overall percent necrosis observed in mice treated with PTX–PEG–ALN conjugate. On the contrary, a significant necrotic core in the ossea medulla was observed only in mice treated with the conjugate, whereas in control mice tumor within the ossea medulla was viable with no necrosis observed (Fig. 7F). Immunohistochemical analysis of paraffin-embedded sections of CD34 staining revealed that in mice treated with PTX–PEG–ALN conjugate there was a significant reduction of ~73% in the MVD (Fig. 7G).

4. Discussion

In this study, we describe the development of a non-toxic formulation of PTX, as bone-targeted antitumor and anti-angiogenic drug. PTX was chosen because it is a highly potent anticancer agent [7,32–35]. In our approach, we aim to target PTX selectively to breast cancer bone metastases while avoiding the side effects entailed by the free drug.

Unlike free PTX, which is only dissolved in organic solvents, PTX–PEG–ALN is soluble in water. Conjugation with the targeting agent ALN provided the selective delivery to bones [15,36], whereas the conjugation with PEG polymer delivered the drugs selectively to tumor sites within bones due to their large size and the EPR effect [22]. PTX was conjugated with a dendron of PEG in which all building blocks of the conjugate are non-toxic. Indeed, as demonstrated previously, PTX–PEG–ALN conjugate had no hemolytic activity at up to 5 mg/ml in an *ex vivo* RBC lysis assay [29].

From the point of view of chemical structure, the heterobifunctional PEG, used in this study, allows the obtainment of conjugates with a high degree of homogeneity. In fact, the targeting and cytotoxicity functionalities can be separated by coupling ALN and PTX at the opposite end chains of the polymer. This structural organization separates also the hydrophobic PTX from the hydrophilic ALN, favoring the formation of micelles presenting the ALN molecules on the surface ready for hydroxyapatite binding.

PTX, when bound with PEG, showed similar cytotoxicity to 4T1 and MDA-MB-231 cells compared with free PTX, suggesting that PTX can be released from the conjugates and achieve similar tumor cells killing efficacy. Inhibition of proliferation, capillary-like tube formation, and migration of endothelial cells revealed that both PTX–PEG and PTX–PEG–ALN conjugates possesses anti-angiogenic properties and are as potent as the free drugs at equivalent concentrations.

Biodistribution analysis demonstrated preferred accumulation in tumors in all FITC-labeled conjugates following 8 h of injection, possibly as a result of the EPR effect. PTX–PEG–ALN–FITC conjugate accumulated mostly in the tumors. This enhanced accumulation was designed to be reinforced by dual targeting of the EPR effect and the addition of the targeting molecule, ALN. Surprisingly, also PEG–ALN–FITC preferentially accumulated in bones rather than in tumor within the bone, as compared with PTX–PEG–ALN–FITC. For PEG–ALN–FITC, targeting with ALN was more dominant than targeting through the EPR effect, this might be related with the lower molecular weight of PEG–ALN (not forming self-assembled micellar structures as in the presence of PTX which assembles as a hydrophobic core). An explicit accumulation in the kidneys of all conjugates is due to renal excretion that is profound 8 h following injection of the conjugates.

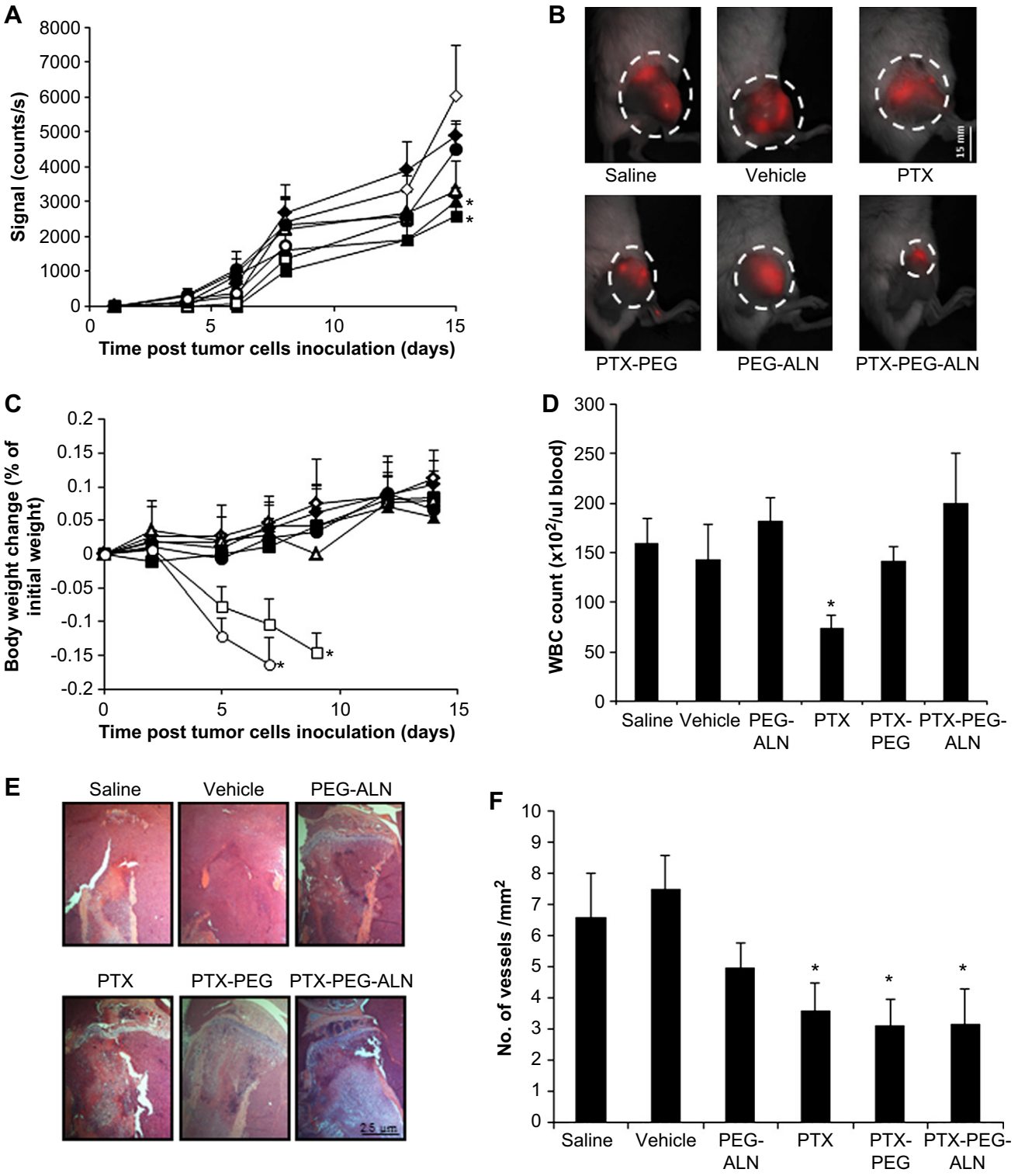

Fig. 5. PTX–PEG–ALN conjugate inhibits mCherry-4T1 adenocarcinoma of the mammary in the tibia. Mice bearing mCherry-4T1 tumors in the tibia were administered *i.v.*, every other day with 15 mg/kg PTX (open triangles), 35 mg/kg ALN (open circles), the combination of free ALN plus PTX (open squares), PTX–PEG (close triangles), PEG–ALN (close circles), PTX–PEG–ALN (close squares) conjugates at equivalent concentrations and with saline (close diamonds) or PTX-vehicle (open diamonds) that were used as controls. (A) Antitumor efficacy measured by intravital non-invasive fluorescence imaging of mCherry-4T1 tumors in the tibia. (B) Fluorescence images of mCherry-4T1 tumors in the tibia. (C) Percent body weight change from initial weight. (D) WBC counts from blood samples collected on day 11. (E) H & E of tumor sections of control, free PTX, and conjugates-treated mCherry-4T1 tumors in the tibia. (F) MVD assessed by vascular marker CD34 staining. $^{*}P < 0.05$ value of mice treated with PEG conjugates was analyzed against saline treated mice, *P* value of free PTX was analyzed against control mice treated with PTX-vehicle. Data represent mean ± s.e.m. ($n = 6$ mice per group).

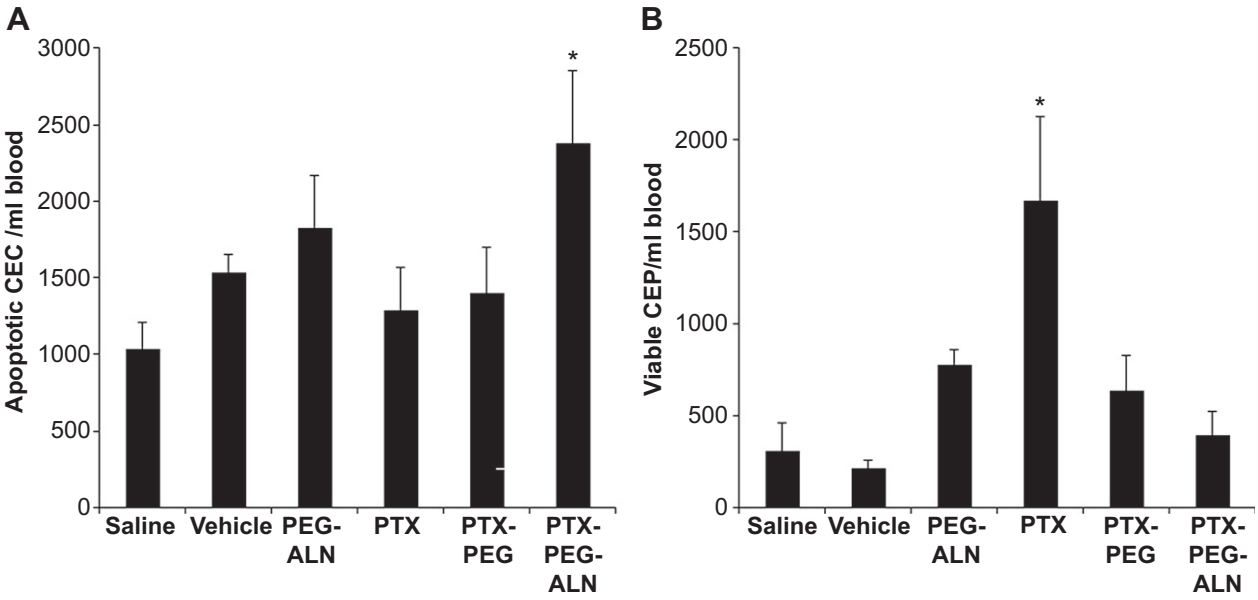

Fig. 6. PTX–PEG–ALN conjugate increases the apoptotic CEC counts. Mice bearing mCherry-4T1 tumors in the tibia were administered *i.v.*, every other day with 15 mg/kg PTX, 35 mg/kg ALN, the combination of free ALN plus PTX, PTX–PEG, PEG–ALN, PTX–PEG–ALN conjugates at equivalent concentrations and with saline or PTX-vehicle that were used as controls. On day 11, blood samples were collected and apoptotic CEC and viable CEP levels were measured using flow cytometry analysis. Quantitative flow cytometry analysis of apoptotic CEC (A) and viable CEP (B). The calculation of the number of apoptotic CEC and viable CEP in peripheral blood was based on the WBC of each mouse. $^{*}P < 0.05$ value of mice treated with PEG–PTX–ALN conjugate was analyzed against saline control mice. Data represent mean ± s.e.m. ($n = 6$ mice per group).

PTX–PEG–ALN conjugate showed substantial antitumor effects in both murine syngeneic and human xenograft mouse models. Additionally, the superiority of the conjugate is evident in its safety compared to the free drugs. In both mouse models, treatment with the combination of free PTX plus ALN caused mortality within the first injection. Even treatment with free PTX plus ALN at half-dose was very toxic and caused a reduction of 20% in body weight, whereas treatment with PTX–PEG–ALN conjugate did not. Also, in contrast to free ALN, mice treated with PEG–ALN conjugate did not lose weight, suggesting that the conjugation with PEG increased the safety of ALN without hindering its bone-targeting affinity. While free ALN diffuses through the blood vessels and affects normal healthy tissues besides the bones, and causes toxicity, the conjugate is targeted only to the bones where there are leaky vessels, i.e. tumor angiogenesis.

WBC levels in mice treated with the conjugate were comparable to those in control mice, whereas mice treated with free PTX, displayed a significant decrease in WBC levels. These results indicate that the conjugation of PTX with PEG and ALN is able to rescue the bone marrow from the toxic effect of free PTX.

H & E staining for both mCherry-4T1- and mCherry-MDA-MB-231 showed intact bone in mice treated with PTX–PEG–ALN conjugate. However, in control mice, bones were destroyed, and tumor penetrated into the proximal soft tissues and the proximal joint. Although overall percent necrosis was increased in control treated mice, as compared to mice treated with the conjugate, a specific larger necrotic area was observed in the ossea medulla of conjugate-treated mice. These findings suggest that the conjugate, as designed, is targeted into bone, and is active in the bones. H & E staining of PEG–ALN-treated mice showed more preserved bones, as compared with saline-treated control mice. These results are surprising with respect to the fact that PEG–ALN did not inhibit tumor growth. Probably the ALN molecule when bound with PEG preserved the bone and prevented bone fractures.

Immunohistochemical staining with CD34 carried out on 4T1 and MDA-MB-231 tumor sections showed that PTX–PEG–ALN conjugate is also directed against tumor endothelial cells and inhibits angiogenesis. These results suggest that the antitumor effect caused by PTX–PEG–ALN conjugate is further mediated by impairing the blood supply to the tumor beyond its direct activity on the tumor cells. This data is supported by the *in vitro* anti-angiogenic activity presented by the conjugate and the *in vivo* evaluation of the angiogenic cellular markers, apoptotic CEC, and viable CEP. Previous work showed that viable CEP correlate with angiogenesis, substantial increase in the number of viable CEP was observed in peripheral blood of mice 24 h after they were treated with PTX [30,37]. Such cells were found in large numbers in treated tumor sites, and thus may account for the induction in angiogenesis and tumor re-growth following therapy [37]. In addition, apoptotic CEC are likely to represent an indirect marker of vessel damage and/or turnover and remodeling [38,39]. We observed an increase in the apoptotic CEC levels only in 4T1 tumor-bearing mice treated with PTX–PEG–ALN conjugate and induction in viable CEP only in the free PTX group, when compared to all other treatments. These findings suggest that the late pro-angiogenic effects that were demonstrated by induction in CEP levels following treatment with PTX can be diminished by PTX–PEG–ALN treatment [37].

We further demonstrate that increased levels of apoptotic CECs correlated with anti-tumor activity, as shown by several studies both at the preclinical and clinical levels. In a study by Mancuso et al. [40] a preclinical study conducted on mice administered with escalating doses of chemotherapy (in a metronomic regimen), a correlation between the anti-tumor activity and increased levels of apoptotic CECs in the blood of these mice was found in both breast cancer and melanoma tumors. However, when such experiments were conducted on non-tumor bearing mice, there was no evidence for increased levels of apoptotic CECs. These results suggest that the apoptotic endothelial cells found in the blood circulation of tumor-bearing mice are actually a result of blood vessel regression in the effectively-treated tumor. In the same study, levels of apoptotic CECs in breast cancer patients who received chemotherapy (in a metronomic regimen) of cyclophosphamide with thalidomide and methotrexate were also evaluated. It was

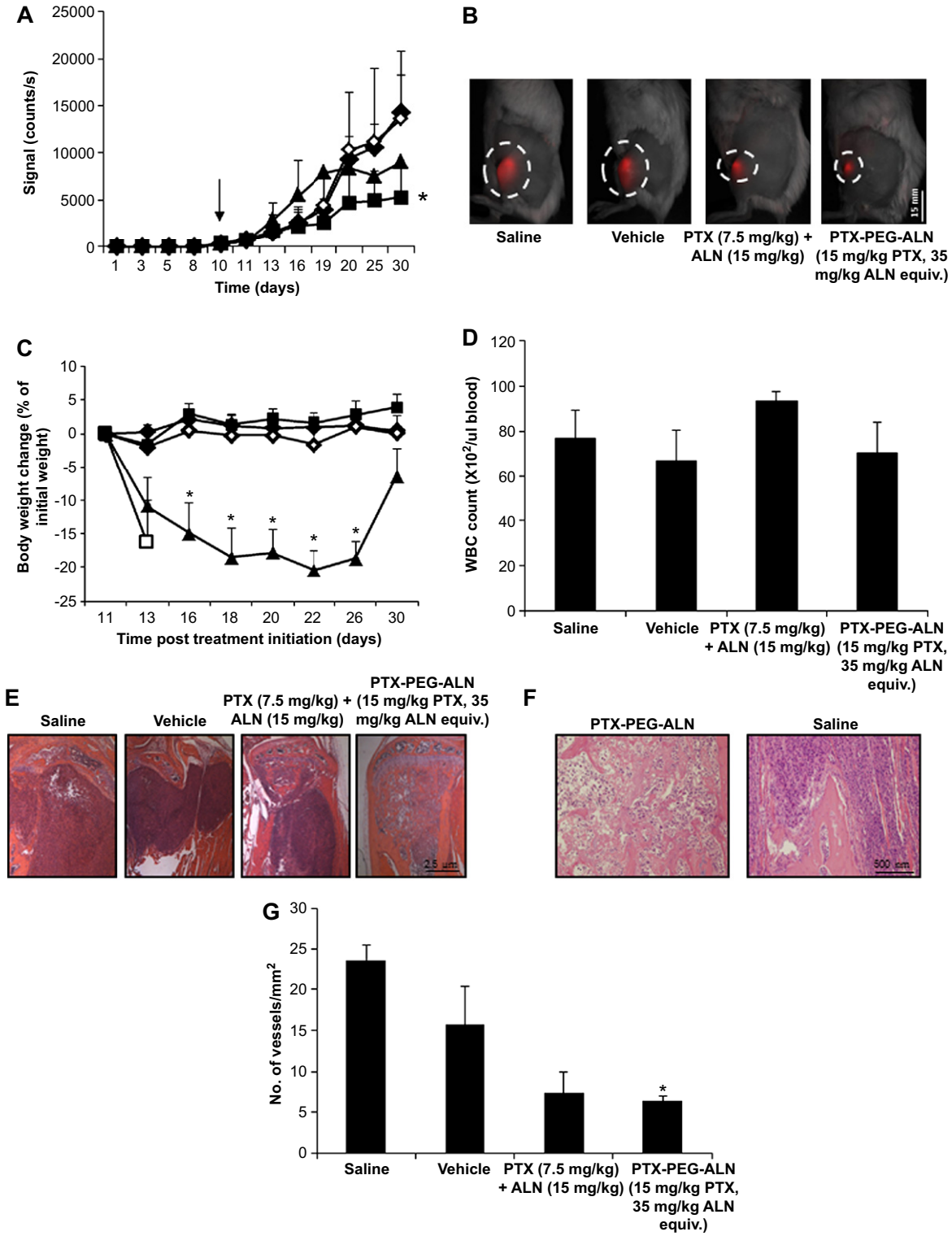

Fig. 7. PTX–PEG–ALN conjugate inhibits mCherry-MDA-MB-231 adenocarcinoma of the mammary tumors in the tibia. Mice bearing mCherry-MDA-MB-231 tumors in the tibia were administered *i.v.*, every other day with the combination of free 35 mg/kg ALN plus 15 mg/kg PTX (open squares), the combination of free 17.5 mg/kg ALN plus 7.5 mg/kg PTX (close triangles), PTX–PEG–ALN conjugate (close squares) (dose: 15 mg/kg PTX and 35 mg/kg ALN equiv.), and with saline (close diamonds) or PTX-vehicle (open diamonds) that were used as controls. (A) Antitumor efficacy measured by intravital non-invasive fluorescence imaging of mCherry-MDA-MB-231 tumors in the tibia. (B) Fluorescence images of mCherry-MDA-MB-231 tumors in the tibia. (C) Percent body weight change from initial weight. (D) WBC counts from blood samples collected on day 20. (E) H & E, staining of tumor sections of control, free combination of PTX, and PTX–PEG–ALN conjugate treated mCherry-labeled MDA-MB-231 tumors in the tibia. (F) H & E staining of ossea medulla tumor sections of saline and PTX–PEG–ALN treated mice. (G) MVD assessed by vascular marker CD34 staining. Data represent mean ± s.e.m. ($n = 6$ mice per group). $^{*}P < 0.05$ value of mice treated with PTX–PEG–ALN conjugate was analyzed against saline treated mice, *P* value of combination of free PTX plus ALN was analyzed against control mice treated with PTX-vehicle.

found that in the patients who respond to therapy (stable disease, partial or complete response) the levels of apoptotic CECs was significantly higher when compared to patients who did not respond to such therapy. Once again, these results suggest that increased levels of apoptotic CECs correlated with clinical outcome (and tumor shrinkage) both clinically and pre-clinically. Furthermore, in line with this specific study, two other clinical studies have shown a correlation between apoptotic CECs and increased survival of cancer patients following therapy [41,42]. Overall, apoptotic CECs appear to serve as a possible biomarker for treatment outcome.

Overall, our data indicate that PTX–PEG–ALN represents potential treatment with a greater anti-angiogenic activity when compared to free PTX. When comparing with PTX–PEG conjugate, that significantly improved efficacy and reduced toxicity as well, one can speculate that the addition of the ALN with PTX–PEG conjugate did not improve much the performance of the conjugate. However, based on the H & E staining demonstrating increased areas of intact bone following treatment with PTX–PEG–ALN, the biodistribution studies showing better tumor accumulation, and the paramount effect on CEP levels, we speculate that targeting with ALN is beneficial in the long-term and can be better-tolerated by patients by way of preserving the bone integrity.

5. Conclusions

We demonstrated a concept of a combined polymer therapeutic designed to target bone metastases by co-delivery of two synergistic drugs at a single administration. PTX–PEG–ALN nano-conjugate was designed and evaluated *in vitro* and *in vivo* as a non-toxic bone-targeted antitumor and anti-angiogenic drug. PEG conjugation allowed PTX–PEG–ALN to be soluble in water, unlike free PTX, and self-assemble in the form of micelles, where the hydrophobic PTX is encapsulated in the core and the hydrophilic ALN is presented on the surface ready for hydroxyapatite binding. PTX was released from the conjugate and had similar tumor cell-killing efficacy as free PTX. PTX–PEG–ALN nano-conjugate possesses anti-angiogenic properties as demonstrated by inhibition of proliferation, capillary-like tube formation, and migration of endothelial cells. PTX–PEG–ALN nano-conjugate selectively accumulated in tumors and displayed substantial anti-tumor effects in both murine syngeneic and human xenogeneic mouse models of bone metastases of mammary carcinomas. The conjugate showed improved safety compared to the free drugs. Treatment with PTX–PEG–ALN nano-conjugate was able to preserve the intact bone structure, while in control mice, bones were destroyed, and tumor penetrated into the proximal soft tissues and the proximal joint.

Acknowledgments

This study was supported (in part) by grant no. 5145-300000 from the Chief Scientist Office of the Ministry of Health, Israel, by THE ISRAEL SCIENCE FOUNDATION (grant No. 1309/10), Grant No. 2007347 given by the United States-Israel Binational Science Foundation (BSF), Swiss Bridge Award, The Israel Cancer Research Fund (ICRF) (RSF) and by The Italian Ministry of Education University and Research (MIUR; grant No. 60A04-3953/10) (GP). We are grateful to the Marian Gertner Institute for Medical Nanosystems and The Cancer Biology Research Center for a Ph.D. fellowship (KM, AEB). This work was also supported by ISF and Marie Curie (under the FP7 EU program) given to YS. LB is supported by Fine, Jacobs and Israel Student Education Foundation studentships.

Appendix A. Supplementary data

Supplementary data related to this article can be found at http://dx.doi.org/10.1016/j.biomaterials.2013.01.052.

References

[1] Parkin DM, Bray F, Ferlay J, Pisani P. Global cancer statistics, 2002. CA Cancer J Clin 2005;55(2):74–108.
[2] Demicheli R, Valagussa P, Bonadonna G. Does surgery modify growth kinetics of breast cancer micrometastases? Br J Cancer 2001;85(4):490–2.
[3] Hansen E, Wolff N, Knuechel R, Ruschoff J, Hofstaedter F, Taeger K. Tumor cells in blood shed from the surgical field. Arch Surg 1995;130(4):387–93.
[4] Colleoni M, O'Neill A, Goldhirsch A, Gelber RD, Bonetti M, Thurlimann B, et al. Identifying breast cancer patients at high risk for bone metastases. J Clin Oncol 2000;18(23):3925–35.
[5] Yoneda T. Cellular and molecular basis of preferential metastasis of breast cancer to bone. J Orthop Sci 2000;5(1):75–81.
[6] Horwitz SB, Cohen D, Rao S, Ringel I, Shen HJ, Yang CP. Taxol: mechanisms of action and resistance. J Natl Cancer Inst Monographs 1993;15:55–61.
[7] Bhalla KN. Microtubule-targeted anticancer agents and apoptosis. Oncogene 2003;22(56):9075–86.
[8] Wang J, Lou P, Lesniewski R, Henkin J. Paclitaxel at ultra low concentrations inhibits angiogenesis without affecting cellular microtubule assembly. Anticancer Drugs 2003;14(1):13–9.
[9] Pasquier E, Carre M, Pourroy B, Camoin L, Rebai O, Briand C, et al. Antiangiogenic activity of paclitaxel is associated with its cytostatic effect, mediated by the initiation but not completion of a mitochondrial apoptotic signaling pathway. Mol Cancer Ther 2004;3(10):1301–10.
[10] Weiss RB, Donehower RC, Wiernik PH, Ohnuma T, Gralla RJ, Trump DL, et al. Hypersensitivity reactions from taxol. J Clin Oncol 1990;8(7):1263–8.
[11] Gelderblom H, Verweij J, Nooter K, Sparreboom A. Cremophor EL: the drawbacks and advantages of vehicle selection for drug formulation. Eur J Cancer 2001;37(13):1590–8.
[12] Caraglia M, Santini D, Marra M, Vincenzi B, Tonini G, Budillon A. Emerging anti-cancer molecular mechanisms of aminobisphosphonates. Endocr Relat Cancer 2006;13(1):7–26.
[13] Fournier P, Boissier S, Filleur S, Guglielmi J, Cabon F, Colombel M, et al. Bisphosphonates inhibit angiogenesis in vitro and testosterone-stimulated vascular regrowth in the ventral prostate in castrated rats. Cancer Res 2002;62(22):6538–44.
[14] Sevcik MA, Luger NM, Mach DB, Sabino MA, Peters CM, Ghilardi JR, et al. Bone cancer pain: the effects of the bisphosphonate alendronate on pain, skeletal remodeling, tumor growth and tumor necrosis. Pain 2004;111(1–2):169–80.
[15] Wang D, Miller S, Sima M, Kopeckova P, Kopecek J. Synthesis and evaluation of water-soluble polymeric bone-targeted drug delivery systems. Bioconjug Chem 2003;14(5):853–9.
[16] Uludag H. Bisphosphonates as a foundation of drug delivery to bone. Curr Pharm Des 2002;8(21):1929–44.
[17] Wang D, Miller SC, Kopeckova P, Kopecek J. Bone-targeting macromolecular therapeutics. Adv Drug Deliv Rev 2005;57(7):1049–76.
[18] Hirabayashi H, Fujisaki J. Bone-specific drug delivery systems: approaches via chemical modification of bone-seeking agents. Clin Pharm 2003;42(15):1319–30.
[19] Segal E, Pan H, Ofek P, Udagawa T, Kopeckova P, Kopecek J, et al. Targeting angiogenesis-dependent calcified neoplasms using combined polymer therapeutics. PLoS One 2009;4(4):e5233.
[20] Miller K, Erez R, Segal E, Shabat D, Satchi-Fainaro R. Targeting bone metastases with a bispecific anticancer and antiangiogenic polymer-alendronate-taxane conjugate. Angew Chem Int Ed Engl 2009;48(16):2949–54.
[21] Miller K, Eldar-Boock A, Polyak D, Segal E, Benayoun L, Shaked Y, et al. Antiangiogenic antitumor activity of HPMA copolymer-paclitaxel-alendronate conjugate on breast cancer bone metastasis mouse model. Mol Pharmacol 2011;8(4):1052–62.
[22] Maeda H, Wu J, Sawa T, Matsumura Y, Hori K. Tumor vascular permeability and the EPR effect in macromolecular therapeutics: a review. J Control Release 2000;65(1–2):271–84.
[23] Pasut G, Veronese FM. PEG conjugates in clinical development or use as anticancer agents: an overview. Adv Drug Deliv Rev 2009;61(13):1177–88.
[24] Duncan R. Polymer conjugates as anticancer nanomedicines. Nat Rev Cancer 2006;6(9):688–701.
[25] Duncan R. Designing polymer conjugates as lysosomotropic nanomedicines. Biochem Soc Trans 2007;35(Pt. 1):56–60.
[26] Satchi-Fainaro R. Targeting tumor vasculature: reality or a dream? J Drug Target 2002;10(7):529–33.
[27] Santucci L, Mencarelli A, Renga B, Ceccobelli D, Pasut G, Veronese FM, et al. Cardiac safety and antitumoral activity of a new nitric oxide derivative of pegylated epirubicin in mice. Anticancer Drugs 2007;18(9):1081–91.
[28] Pasut G, Greco F, Mero A, Mendichi R, Fante C, Green RJ, et al. Polymer-drug conjugates for combination anticancer therapy: investigating the mechanism of action. J Med Chem 2009;52(20):6499–502.

[29] Clementi C, Miller K, Mero A, Satchi-Fainaro R, Pasut G. Dendritic poly(ethylene glycol) bearing paclitaxel and alendronate for targeting bone neoplasms. Mol Pharmacol 2011;8(4):1063–72.
[30] Shaked Y, Bertolini F, Man S, Rogers MS, Cervi D, Foutz T, et al. Genetic heterogeneity of the vasculogenic phenotype parallels angiogenesis: implications for cellular surrogate marker analysis of antiangiogenesis. Cancer Cell 2005; 7(1):101–11.
[31] Weidner N, Semple JP, Welch WR, Folkman J. Tumor angiogenesis and metastasis–correlation in invasive breast carcinoma. N Engl J Med 1991; 324(1):1–8.
[32] Arbuck SG, Dorr A, Friedman MA. Paclitaxel (Taxol) in breast cancer. Hematol Oncol Clin North Am 1994;8(1):121–40.
[33] Cetnar JP, Malkowicz SB, Palmer SC, Wein AJ, Vaughn DJ. Pilot trial of adjuvant paclitaxel plus estramustine in resected high-risk prostate cancer. Urology 2008;71(5):942–6.
[34] Hennenfent KL, Govindan R. Novel formulations of taxanes: a review. Old wine in a new bottle? Ann Oncol 2006;17(5):735–49.
[35] Sanfilippo NJ, Taneja SS, Chachoua A, Lepor H, Formenti SC. Phase I/II study of biweekly paclitaxel and radiation in androgen-ablated locally advanced prostate cancer. J Clin Oncol 2008;26(18):2973–8.
[36] Wang D, Sima M, Mosley RL, Davda JP, Tietze N, Miller SC, et al. Pharmacokinetic and biodistribution studies of a bone-targeting drug delivery system based on N-(2-hydroxypropyl)methacrylamide copolymers. Mol Pharmacol 2006;3(6):717–25.
[37] Shaked Y, Henke E, Roodhart JM, Mancuso P, Langenberg MH, Colleoni M, et al. Rapid chemotherapy-induced acute endothelial progenitor cell mobilization: implications for antiangiogenic drugs as chemosensitizing agents. Cancer Cell 2008;14(3):263–73.
[38] Bertolini F, Mancuso P, Braidotti P, Shaked Y, Kerbel RS. The multiple personality disorder phenotype(s) of circulating endothelial cells in cancer. Biochim Biophys Acta 2009;1796(1):27–32.
[39] Bertolini F, Shaked Y, Mancuso P, Kerbel RS. The multifaceted circulating endothelial cell in cancer: towards marker and target identification. Nat Rev Cancer 2006;6(11):835–45.
[40] Mancuso P, Colleoni M, Calleri A, Orlando L, Maisonneuve P, Pruneri G, et al. Circulating endothelial-cell kinetics and viability predict survival in breast cancer patients receiving metronomic chemotherapy. Blood 2006;108(2):452–9.
[41] Glade Bender JL, Adamson PC, Reid JM, Xu L, Baruchel S, Shaked Y, et al. Phase I trial and pharmacokinetic study of bevacizumab in pediatric patients with refractory solid tumors: a Children's Oncology Group Study. J Clin Oncol 2008; 26(3):399–405.
[42] Dellapasqua S, Bertolini F, Bagnardi V, Campagnoli E, Scarano E, Torrisi R, et al. Metronomic cyclophosphamide and capecitabine combined with bevacizumab in advanced breast cancer. J Clin Oncol 2008;26(30):4899–905.